Tunnel and electrostatic coupling in graphene-$LaAlO_3$/$SrTiO_3$ hybrid systems

I. Aliaj' , I. Torre, V. Miseikis, E. di Gennaro, A. Sambri, A. Gamucci, C. Coletti, F. Beltram, F. M. Granozio, M. Polini, V. Pellegrini, and S. Roddaro'

Citation: APL Mater. **4**, 066101 (2016); doi: 10.1063/1.4953821
View online: http://dx.doi.org/10.1063/1.4953821
View Table of Contents: http://aip.scitation.org/toc/apm/4/6
Published by the American Institute of Physics

Tunnel and electrostatic coupling in graphene-$LaAlO_3$/$SrTiO_3$ hybrid systems

I. Aliaj,[1,a] I. Torre,[1] V. Miseikis,[2] E. di Gennaro,[3] A. Sambri,[3] A. Gamucci,[4] C. Coletti,[2,4] F. Beltram,[5] F. M. Granozio,[3] M. Polini,[1,4] V. Pellegrini,[4] and S. Roddaro[5,b]

[1]*NEST, Scuola Normale Superiore, 56127 Pisa, Italy*
[2]*Center for Nanotechnology Innovation @NEST, Istituto Italiano di Tecnologia, Piazza San Silvestro 12, 56127 Pisa, Italy*
[3]*CNR-SPIN and Dipartimento di Fisica, Complesso Universitario di Monte S.Angelo, Via Cintia, 80126 Naples, Italy*
[4]*Istituto Italiano di Tecnologia, Graphene Labs, Via Morego 30, I-16163 Genova, Italy*
[5]*NEST, Istituto Nanoscienze-CNR and Scuola Normale Superiore, 56127 Pisa, Italy*

(Received 12 February 2016; accepted 31 May 2016; published online 9 June 2016)

We report on the transport properties of hybrid devices obtained by depositing graphene on a $LaAlO_3/SrTiO_3$ oxide junction hosting a 4 nm-deep 2-dimensional electron system. At low graphene-oxide inter-layer bias, the two electron systems are electrically isolated, despite their small spatial separation. A very efficient reciprocal gating of the two neighboring 2-dimensional systems is shown. A pronounced rectifying behavior is observed for larger bias values and ascribed to the interplay between electrostatic field-effects and tunneling across the $LaAlO_3$ barrier. The relevance of these results in the context of strongly coupled bilayer systems is discussed. [http://dx.doi.org/10.1063/1.4953821]

Graphene is widely investigated in view of possible device applications owing to its excellent, electric-field tunable electronic properties,[1] its chemical and structural robustness, its ease of production and integrability with a plethora of other material systems.[2] In addition, because of its single-atom thickness, its properties can be very sensitive to the local environment. In particular, interaction with the host substrate offers new ways to tune the properties of graphene and the case of functional transition metal oxides is of significant interest. For instance, graphene field-effect transistors (FETs) built on ferroelectric $Pb(Zr,Ti)O_3$ substrates display pronounced memory effects, ultra-low voltage operation,[3] and open the way to novel nanoplasmonic devices.[4] Similarly, graphene photo-sensitivity was shown to increase 25 times on TiO_2 substrates[5] and intriguing magnetic phenomena are actively pursued in devices combining graphene with EuO substrates[6] or magnetic $La_xSr_{1-x}MnO_3$ electrodes.[7]

In the family of transition metal oxides, interfaces between the bulk band insulators $LaAlO_3$ (LAO) and $SrTiO_3$ (STO) occupy a special place due to their multiple, electric-field tunable properties, such as conductivity,[8,9] superconductivity,[10,11] magnetism,[12,13] and spin-orbit coupling.[14] These phenomena stem from the emergence of an interfacial two-dimensional electron system (2DES) when more than 3 unit cells (u.c.) of LAO are grown on a TiO_2-terminated STO crystal. Such 2DES is located only a few nm below the surface and its properties are therefore extremely sensitive to other materials deposited on this surface, such as metals[15] or other oxides.[16] In this scenario, hybrid structures combining graphene with LAO/STO junctions represent an exciting platform in which novel phenomena may emerge from coupling effects between the respective 2DESs.

[a]Electronic address: ilirjan.aliaj@sns.it
[b]Electronic address: stefano.roddaro@sns.it

In particular, collective interlayer-correlated phases driven by the strong Coulomb interactions could result at low temperatures, in analogy to what observed in graphene/GaAs/AlGaAs systems.[17] Furthermore, different magnetic or superconducting properties may be induced in graphene due to the proximity interaction with the ordered phases of the interfacial 2DES. In order to enable the exploration of these possibilities, the necessary starting point is a clear understanding of the transport behavior of these hybrid systems. LAO/STO-graphene systems, however, have been so far little studied. In a recent paper,[18] graphene was integrated with insulating LAO/STO substrates with subcritical LAO thickness, where a scanning probe microscope was used to "write" nanometer-wide conductive regions on the oxide system[19] and graphene was used as a gate electrode controlling the conduction of these nanowires at the LAO/STO interface.

Here we report on extended ($\approx 10^4$ μm^2) junctions between monolayer graphene grown by chemical vapor deposition (CVD) and a conductive, 4 nm-deep LAO/STO interface hosting a 2DES. Our results demonstrate that strong electrostatic coupling with virtually no leakage can be obtained at room-temperature (RT) between a two-dimensional hole gas in graphene and the LAO/STO 2DES, as long as the graphene-oxide bias V_{GO} is sufficiently small ($|V_{GO}| \lesssim 1$ V). At larger values of $|V_{GO}|$, we report strongly non-linear transport across the vertical graphene-LAO/STO junction that will be linked to tunneling currents between the two electron systems.

The device structure adopted in this work is illustrated in Fig. 1. High-quality 2DESs were obtained by growing 10 u.c.-thick LAO films on TiO_2-terminated STO chips by pulsed laser deposition.[20] Cr/Au alignment markers were fabricated by e-beam lithography and thermal evaporation and no additional processing was carried out in order to minimize contamination and damage of

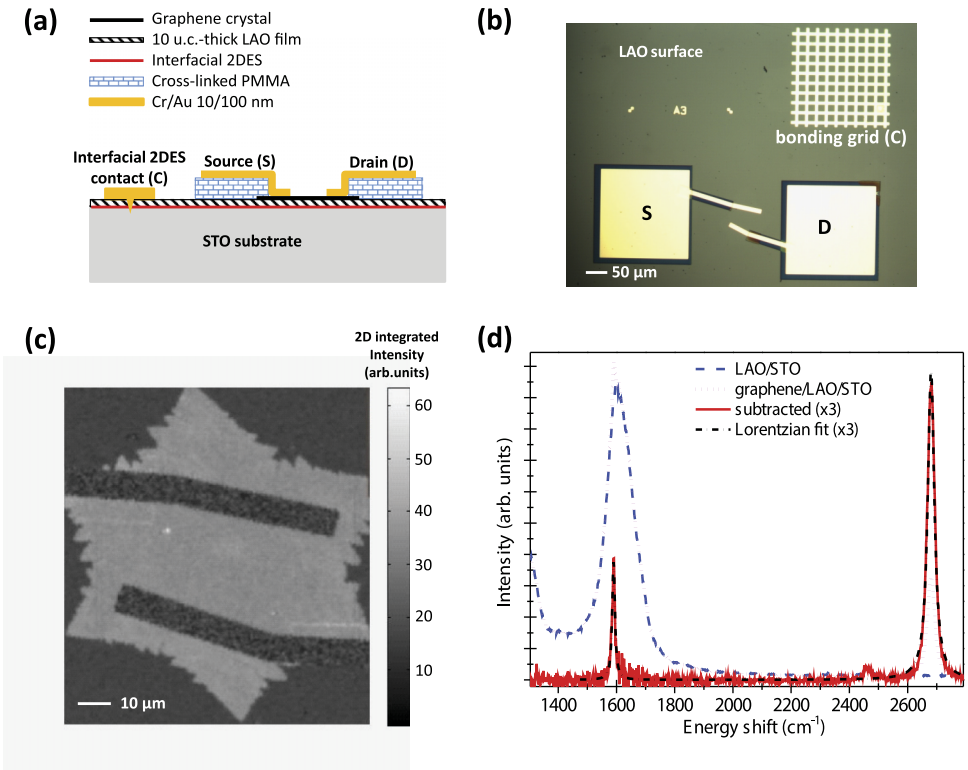

FIG. 1. Monolayer of CVD graphene crystal deposited on LAO/STO. (a) Sketch of the device architecture and (b) optical image of a representative three-terminal graphene/LAO/STO device for electrical transport studies at room temperature. Raman microspectrocopy of the contacted CVD graphene monocrystal in a fabricated device, showing the (c) map of the integrated intensity of the 2D peak and the (d) Raman spectroscopic analysis of the graphene crystal. The substrate-free graphene spectrum (red line) was obtained by subtracting Raman spectra acquired on regions covered by/free of graphene (dotted pink/dashed blue); the spectrum is compatible with a single layer crystal and the absence of D peak reveals that graphene's good quality is maintained during the fabrication procedure.

the oxide system. Single-crystalline graphene flakes typically measuring 100 μm in diameter were grown by CVD on flat, *ex situ* passivated Cu foils.[21] Graphene crystals were finally deposited on the clean surfaces of LAO/STO heterostructures using a polymer-based transfer process[22] and localized, thanks to the Cr/Au markers. The device architecture was designed taking particular care to avoid spurious electrical losses across the ≈4 nm-thick LAO barrier. An insulating layer of 200 nm of cross-linked PMMA was inserted between the LAO/STO and graphene electrodes (see the sketch of Fig. 1(a) and the optical picture of Fig. 1(b)), so that the only electrical path between the contact leads and the LAO/STO 2DES occurred vertically through the graphene-LAO/STO junction. The correct alignment of the flakes and their quality at the end of the process were assessed through Raman spectroscopy, as shown in Figs. 1(c) and 1(d) for one of the studied devices. Given the relatively strong background signal from the LAO/STO substrate, Raman spectra were processed by subtracting the response of the bare oxide heterostructure (see Fig. 1(d)). Once this background signal was removed, Raman emission clearly indicated that the graphene flake was a high-quality monolayer, with a single-Lorentzian 2D peak, the expected G/2D peak ratio for monolayer graphene and no discernible D peak throughout the crystal.[23] The correct alignment and uniformity of the flake is demonstrated in Fig. 1(c), where we report a Raman map integrated over the spectral region 2600–2800 cm^{-1} corresponding to the 2D peak.

Device parameters and structure were chosen to achieve strong electrostatic coupling between the 2DESs in graphene and in the LAO/STO heterojunction, with negligible tunneling in the small interlayer bias (V_{GO}) limit. Based on electron affinity values,[24] we estimate a large (>2 eV) graphene-LAO barrier (see Fig. 2(a)) that should electrically decouple the two electronic systems. At present many of the band parameters of the junction, in particular the exact band offsets and, consequently, the built-in field in the LAO layer, are still debated [Refs. 25 and 26, and references therein]. In addition, the triangular quantum well potential at the LAO/STO interface confines the motion of oxide electrons to a non-trivial set of 2D subbands characterized by different and anisotropic effective masses.[27–29] In the following, the interface 2DES will be simply described by a single isotropic 2D subband and charge transport between the two 2DESs will be assumed to occur via direct tunneling across the ≈4 nm LAO barrier. The electrostatic coupling between the two 2DESs is described in terms of a capacitor in which the electrodes have a finite density of states (DOS), as explained in detail in Section I of the supplementary material.[30]

The typical transport properties of a representative graphene-LAO/STO hybrid device are reported in Fig. 2(b). The insulating properties of the PMMA layer were preliminarily studied on ≈200 × 200 μm^2 test pads covered by unconnected metallic electrodes: negligible ($\lesssim$0.1 nA) vertical currents were observed for vertical biases in the studied V_{GO} range. Graphene devices were measured using a piezo-actuated microprobe system from Imina Technologies in order to avoid inducing electrical loss through the PMMA as a consequence of wire-bonding. We studied the RT vertical transport between the oxide interfacial 2DES and graphene by applying a DC bias V_{GO} to the graphene electrode while holding the interfacial 2DES at ground. As shown in Fig. 2(b), a strongly non-linear transport characteristic was observed, where different regimes can be distinguished. Around zero bias, graphene and the 2DES are insulated and no current could be detected above the noise: a current of few pA is measured for $|V_{GO}| < 0.5$ V, corresponding to a resistance in the range 10 GΩ–100 GΩ. Outside this interval, vertical transport sets on, with an approximately exponential current-voltage characteristic. For $V_{GO} < -2.5$ V, vertical current saturates to a fraction of nA: as discussed in the following, this is due to a field-effect depletion of the oxide interfacial 2DES. The exponential growth is much more pronounced for positive bias values: the current grows by 5 orders of magnitude in less than 1 V of bias change and it is ultimately limited (for $V_{GO} > 1.5$ V) by the resistive load of the 2DES region connecting the junction area to the electrodes.

In the range $V_{GO} = 0.5 - 1.5$ V, referred to as the intrinsic regime, transport is governed only by the vertical junction properties and was therefore amenable to theoretical modeling, as reported in the supplementary material.[30] The observed transport characteristics at positive bias are compatible with direct tunneling of electrons between graphene and the interfacial 2DES. In fact, the large graphene-LAO barrier (>2 eV) suggests that thermionic emission should be suppressed even at RT, while tunneling remains possible because of the ultra-thin barrier. Zener tunneling across the

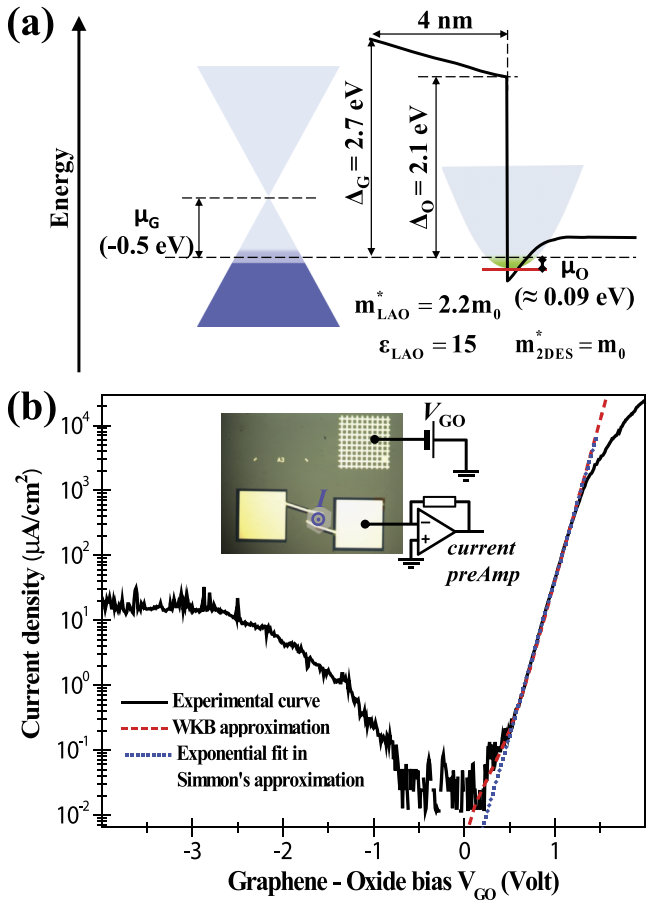

FIG. 2. Pronounced non-linear transport in graphene-LAO/STO systems. (a) Schematic of the conduction band profile of the LAO/STO heterostructure and the relative band alignment between graphene and LAO barrier in equilibrium conditions, illustrating the relevant microscopic parameters of the vertical junction and the corresponding values that best reproduce the experimental transport data. (b) Graphene-oxide 2DES (black solid) current density as a function of vertical bias V_{GO} measured in a representative device at room temperature and the corresponding graphene-2DES tunneling characteristic calculated in the full WKB (red dashed) and Simmon's approximation (blue dotted), as reported in the supplementary material.[30] The inset is a schematic of the electrical setup used for studying the vertical transport properties of the system.

LAO should be negligibly small for 10 u.c.-thick LAO films,[31] particularly for positive values of V_{GO}, which tend to flatten the LAO potential. Therefore, only direct graphene-2DES tunneling was considered and calculated in the semiclassical (WKB) approximation that was already successfully adopted to describe transport features in both metal/LAO/STO[31] and van der Waals heterostructures comprising graphene.[32] Input parameters used to reproduce the experimental data are reported in Fig. 2(a) and were set at the typically reported values in the literature, apart from the barrier effective mass that was obtained by fitting the data in the Simmon's approximation (dotted blue curve in Fig. 2(b)), as explained in Section III of the supplementary material.[30] Fig. 2(b) compares the resulting theoretical prediction (red dashed line) with a typical experimental curve (solid black line): the model is quantitatively accurate in the intrinsic regime, thus providing evidence that graphene-interfacial 2DES transport is indeed dominated by direct tunneling of electrons through the LAO barrier. Finally, we note that similar rectifying behavior was already reported in metal(Pt,Au)/LAO/STO junctions[11,31,33] and was also attributed mainly to quantum tunneling.[31] The similarities are due to the metallic behavior of graphene for large positive values of V_{GO} and the comparable electron affinities of graphene and Pt, Au.

In the low inter-layer bias limit, and for the full range $V_{GO} < 1.0$ V, graphene and the interfacial 2DES can be considered electrically insulated, with vertical currents lower than 0.5 nA. The

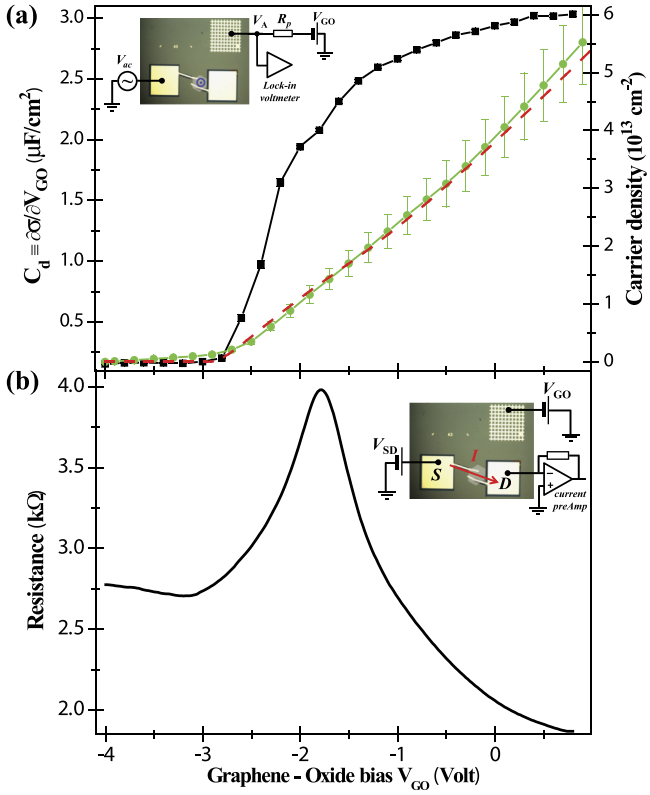

FIG. 3. Strong electrostatic coupling in graphene-LAO/STO systems. (a) Experimentally measured differential capacitance of the vertical junction (black squares) and the deduced interfacial 2DES carrier density (green disks) as a function of vertical bias, showing the pronounced electric-field-effects in the hybrid structure. The red dashed curve represents the density-bias relationship obtained from the electrostatic model. (b) Room temperature 2-point resistance of the single layer graphene crystal as a function of V_{GO}, suggesting the tuning of graphene carrier density across the Dirac point. The insets are schematics of the electrical setups employed for studying the electric-field-effects of the system. The blue and red arrows represent respectively the vertical and in-plane current flow in our device.

existence of this quasi-insulating regime makes it possible to explore Coulomb coupling between the two electron systems.

The prominent electrostatic coupling in our system was corroborated through capacitance-voltage (C-V) measurements, whose main result is shown in Figure 3(a) for a representative device. A large geometrical capacitance of $\approx 3\ \mu F/cm^2$, corresponding to a relative dielectric constant of ≈ 15 for the 10 u.c.-thick LAO film, can be deduced from the positive bias regime ($V_{GO} > 0.5$ V), where the contribution of the graphene and oxide-2DES quantum capacitance becomes negligible. Such a high capacitance follows from the small thickness of the LAO dielectric and implies a strong field-effect in our devices. In fact, the sharp drop of the capacitance at $V_{GO} \approx -2.5$ V demonstrates the depletion of the densely populated interfacial 2DES, also reported in metal(Au,Pt)/LAO/STO junctions.[11,31,33] The creation of a highly insulating area in the junction region of the LAO/STO interface explains the observed saturation of the vertical currents for high negative bias (Fig. 2(b)). Moreover, by numerically integrating the C-V curve from the pinch-off voltage, we are able to reconstruct the evolution of the interfacial 2DES carrier density with vertical bias. The result is shown in Fig. 3(a) in green circles and indicates an unbiased population of $(3.9 \pm 0.4) \times 10^{13}$ cm^{-2} for the oxide 2DES, whose carrier density can be modulated from full depletion at negative bias, up to densities of $\approx 5.5 \times 10^{13}$ cm^{-2} for positive ones. These results are further confirmed by our electrostatic model: the oxide 2DES density-bias relationship predicted by the latter is shown in a red-dashed curve in Fig. 3(a), and it quantitatively reproduces the experimental data and in particular the pinch-off of the latter at high negative bias. A more detailed analysis of the C-V

measurements and its comparison with the electrostatic model is reported in Section I of the supplementary material.[30]

The reciprocal field-effect, i.e., the one of the interfacial 2DES on graphene, was demonstrated by monitoring the 2-point resistance of graphene as a function of V_{GO}: the result is shown in Fig. 3(b) for a representative device and demonstrates the significant modulation of the graphene resistivity by the electric field of the 2DES electrode. The resistance curve indicates that graphene can be easily tuned between p-type and n-type conduction at a V_{GO} value as small as a fraction of a Volt, which confirms the extremely large gating efficiency of the system. Finally, we find negative charge neutrality points in all our devices, suggesting that graphene crystals on LAO/STO substrates are p-doped, as typically observed.

In conclusion, we reported on the transport properties of the graphene-LAO/STO hybrid system and showed that it is characterized by strong electrostatic coupling at low inter-layer bias and direct tunneling coupling at large bias values. Efficient gating could be fruitfully exploited for the realization of hybrid "dual" FETs[34] with very-low operating voltage, where graphene can be employed either as gate, or as the conducting channel back-gated by the 2DES. The present device architecture can be relevant to the investigation of collective phases with very strong inter-layer correlations at low temperatures.

During the submission process, the preprint of another experimental work on graphene-LAO/STO systems[35] appeared, showing that sub-critical (insulating) LAO/STO substrates allow the observation of quantum transport features, such as weak anti-localization and anomalous quantum Hall effect, in graphene even at room temperature.

This work was funded by the European Union Seventh Framework Programme under Grant Agreement No. 604391 Graphene Flagship. S.R. acknowledges the support of CNR through the bilateral CNR-RFBR Project No. 2015-2017.

[1] A. K. Geim and K. S. Novoselov, Nat. Mater. **6**, 183 (2007); A. H. Castro Neto, F. Guinea, N. M. R. Peres, K. S. Novoselov, and A. K. Geim, Rev. Mod. Phys. **81**, 109 (2009).
[2] F. Bonaccorso, A. Lombardo, T. Hasan, Zh. Sun, L. Colombo, and A. C. Ferrari, Mater. Today **15**, 564 (2012).
[3] Y. Zheng, G. X. Ni, S. Bae, C. X. Cong, O. Kahya, C. T. Toh, H. R. Kim, D. Im, T. Yu, J. H. Ahn, B. H. Hong, and B. Ozyilmaz, Europhys. Lett. **93**, 17002 (2011); X. Hong, K. Zou, A. M. DaSilva, C. H. Ahn, and J. Zhu, Solid State Commun. **152**, 1365 (2012).
[4] D. F. Jin, A. Kumar, K. H. Fung, J. Xu, and N. X. Fang, Appl. Phys. Lett. **102**, 201118 (2013).
[5] J. Park, T. Back, W. C. Mitchel, S. S. Kim, S. Elhamri, J. Boeckl, S. B. Fairchild, R. Naik, and A. A. Voevodin, Sci. Rep. **5**, 14374 (2015).
[6] H. X. Yang, A. Hallal, D. Terrade, X. Waintal, S. Roche, and M. Chshiev, Phys. Rev. Lett. **110**, 046603 (2013).
[7] F. Li, T. Li, and X. Guo, ACS Appl. Mater. Interfaces **6**, 1187 (2014); M. Rocci, J. Tornos, A. Rivera-Calzada, Z. Sefrioui, M. Clement, E. Iborra, C. Leon, and J. Santamaria, Appl. Phys. Lett. **104**, 102408 (2014).
[8] A. Ohtomo and H. Y. Hwang, Nature **427**, 423 (2004).
[9] S. Thiel, G. Hammerl, A. Schmehl, C. W. Schneider, and J. Mannhart, Science **313**, 1942 (2006).
[10] N. Reyren, S. Thiel, A. D. Caviglia, L. F. Kourkoutis, G. Hammerl, C. Richter, C. W. Schneider, T. Kopp, A.-S. Rüetschi, D. Jaccard, M. Gabay, D. A. Muller, J.-M. Triscone, and J. Mannhart, Science **317**, 1196 (2007).
[11] P. D. Eerkes, W. G. Van Der Wiel, and H. Hilgenkamp, Appl. Phys. Lett. **103**, 201603 (2013).
[12] A. Brinkman, M. Huijben, M. van Zalk, J. Huijben, U. Zeitler, J. C. Maan, W. G. van der Wiel, G. Rijnders, D. H. A. Blank, and H. Hilgenkamp, Nat. Mater. **6**, 493 (2007).
[13] D. Stornaiuolo, C. Cantoni, G. M. De Luca, R. Di Capua, E. Di Gennaro, G. Ghiringhelli, B. Jouault, D. Marrè, D. Massarotti, F. M. Granozio, I. Pallecchi, C. Piamonteze, S. Rusponi, F. Tafuri, and M. Salluzzo, Nat. Mater. **15**, 278 (2016).
[14] M. B. Shalom, M. Sachs, D. Rakhmilevitch, A. Palevski, and Y. Dagan, Phys. Rev. Lett. **104**, 126802 (2010); A. D. Caviglia, M. Gabay, S. Gariglio, N. Reyren, C. Cancellieri, and J.-M. Triscone, *ibid.* **104**, 126803 (2010).
[15] R. Arras, V. G. Ruiz, W. E. Pickett, and R. Pentcheva, Phys. Rev. B **85**, 125404 (2012); E. Lesne, N. Reyren, D. Doennig, R. Mattana, H. Jaffrès, V. Cros, F. Petroff, F. Choueikani, P. Ohresser, R. Pentcheva, A. Barthélémy, and M. Bibes, Nat. Commun. **5**, 4291 (2014).
[16] B. Förg, C. Richter, and J. Mannhart, Appl. Phys. Lett. **100**, 053506 (2012); M. Huijben, G. Koster, M. K. Kruize, S. Wenderich, J. Verbeeck, S. Bals, E. Slooten, B. Shi, H. J. A. Molegraaf, J. E. Kleibeuker, S. van Aert, J. B. Goedkoop, A. Brinkman, D. H. A. Blank, M. S. Golden, G. van Tendeloo, H. Hilgenkamp, and G. Rijnders, Adv. Funct. Mater. **23**, 5240 (2013); Y. J. Shi, S. Wang, Y. Zhou, H. F. Ding, and D. Wu, Appl. Phys. Lett. **102**, 071605 (2013).
[17] A. Gamucci, D. Spirito, M. Carrega, B. Karmakar, A. Lombardo, M. Bruna, A. C. Ferrari, L. N. Pfeiffer, K. W. West, M. Polini, and V. Pellegrini, Nat. Commun. **5**, 5824 (2014).
[18] M. Huang, G. Jnawali, J.-F. Hsu, S. Dhingra, H. Lee, S. Ryu, F. Bi, F. Ghahari, J. Ravichandran, L. Chen, P. Kim, C.-B. Eom, B. D'Urso, P. Irvin, and J. Levy, APL Mater. **3**, 062502 (2015).
[19] C. Cen, S. Thiel, J. Mannhart, and J. Levy, Science **323**, 1026 (2009).

[20] C. Cantoni, J. Gazquez, F. M. Granozio, M. P. Oxley, M. Varela, A. R. Lupini, S. J. Pennycook, C. Aruta, U. S. di Uccio, P. Perna, and D. Maccariello, Adv. Mater. **24**, 3952 (2012); C. Aruta, S. Amoruso, R. Bruzzese, X. Wang, D. Maccariello, F. M. Granozio, and U. S. di Uccio, Appl. Phys. Lett. **97**, 252105 (2010).
[21] V. Miseikis, D. Convertino, N. Mishra, M. Gemmi, T. Mashoff, S. Heun, N. Haghighian, F. Bisio, M. Canepa, V. Piazza, and C. Coletti, 2D Mater. **2**, 014006 (2015).
[22] Y. Wang, Y. Zheng, X. Xu, E. Dubuisson, Q. Bao, J. Lu, and K. P. Loh, ACS Nano **5**, 9927 (2011); L. Gao, W. Ren, H. Xu, L. Jin, Zh. Wang, T. Ma, L.-P. Ma, Zh. Zhang, Q. Fu, L.-M. Peng, X. Bao, and H.-M. Cheng, Nat. Commun. **3**, 699 (2012).
[23] A. C. Ferrari, J. C. Meyer, V. Scardaci, C. Casiraghi, M. Lazzeri, F. Mauri, S. Piscanec, D. Jiang, K. S. Novoselov, S. Roth, and A. K. Geim, Phys. Rev. Lett. **97**, 187401 (2006); A. C. Ferrari and D. M. Basko, Nat. Nanotechnol. **8**, 235 (2013).
[24] Y.-J. Yu, Y. Zhao, S. Ryu, L. E. Brus, K. S. Kim, and P. Kim, Nano Lett. **9**, 3430 (2009); P. W. Peacock and J. Robertson, J. Appl. Phys. **92**, 4713 (2002).
[25] G. Drera, G. Salvinelli, A. Brinkman, M. Huijben, G. Koster, H. Hilgenkamp, G. Rijnders, D. Visentin, and L. Sangaletti, Phys. Rev. B **87**, 075435 (2013).
[26] U. Treske, N. Heming, M. Knupfer, B. Büchner, E. di Gennaro, A. Khare, U. S. di Uccio, F. M. Granozio, S. Krause, and A. Koitzsch, Sci. Rep. **5**, 14506 (2015).
[27] W. J. Son, E. Cho, B. Lee, J. Lee, and S. Han, Phys. Rev. B **79**, 245411 (2009); Z. S. Popovic, S. Satpathy, and R. M. Martin, Phys. Rev. Lett. **101**, 256801 (2008).
[28] J. R. Tolsma, A. Principi, R. Asgari, M. Polini, and A. H. MacDonald, Phys. Rev. B **93**, 045120 (2016).
[29] M. Salluzzo, J. Cezar, N. Brookes, V. Bisogni, G. De Luca, C. Richter, S. Thiel, J. Mannhart, M. Huijben, A. Brinkman, G. Rijnders, and G. Ghiringhelli, Phys. Rev. Lett. **102**, 166804 (2009); C. Cancellieri, M. L. Reinle-Schmitt, M. Kobayashi, V. N. Strocov, P. R. Willmott, D. Fontaine, P. Ghosez, A. Filippetti, P. Delugas, and V. Fiorentini, Phys. Rev. B **89**, 121412 (2014).
[30] See supplementary material at http://dx.doi.org/10.1063/1.4953821 for a more detailed description of the capacitance-voltage measurements and the electrostatic and transport models of the system and complete description of the experimental and theoretical analysis of the electrostatic problem of the junction and the WKB-tunneling model of the graphene-oxide 2DES transport.
[31] G. Singh-Bhalla, C. Bell, J. Ravichandran, W. Siemons, Y. Hikita, S. Salahuddin, A. F. Hebard, H. Y. Hwang, and R. Ramesh, Nat. Phys. **7**, 80 (2010).
[32] L. Britnell, R. V. Gorbachev, R. Jalil, B. D. Belle, F. Schedin, A. Mishchenko, T. Georgiou, M. I. Katsnelson, L. Eaves, S. V. Morozov, N. M. R. Peres, J. Leist, A. K. Geim, K. S. Novoselov, and L. A. Ponomarenko, Science **335**, 947 (2012).
[33] S. K. Kim, S.-I. Kim, H. Lim, D. S. Jeong, B. Kwon, S.-H. Baek, and J.-S. Kim, Sci. Rep. **5**, 8023 (2015).
[34] C.-C. Tang, M.-Y. Li, L. J. Li, C. C. Chi, and J.-C. Chen, Appl. Phys. Lett. **101**, 202104 (2012).
[35] G. Jnawali, M. Huang, J.-F. Hsu, H. Lee, P. Irvin, C.-B. Eom, B. D'Urso, and J. Levy, e-print arXiv:1602.03128v1.